

Relative Pose Estimation and Fusion of Omnidirectional and Lidar Cameras

Levente Tamas¹, Robert Frohlich², and Zoltan Kato²

¹ Technical University of Cluj-Napoca, Robotics Research Group,
Dorobantilor st. 73, 400609, Romania

² Institute of Informatics, University of Szeged,
P.O. Box 652, H-6701 Szeged, Hungary

Abstract. This paper presents a novel approach for the extrinsic parameter estimation of omnidirectional cameras with respect to a 3D Lidar coordinate frame. The method works without specific setup and calibration targets, using only a pair of 2D-3D data. Pose estimation is formulated as a 2D-3D nonlinear shape registration task which is solved without point correspondences or complex similarity metrics. It relies on a set of corresponding regions, and pose parameters are obtained by solving a small system of nonlinear equations. The efficiency and robustness of the proposed method was confirmed on both synthetic and real data in urban environment.

Keywords: Omnidirectional camera, Lidar, pose estimation, fusion

1 Introduction

There is a considerable research effort invested in autonomous car driving projects both at academic and industrial levels. While for special scenarios, such as highways, there are a number of successful applications, there is still no general solution for complex environments such as urban areas [4,10]. Recent developments in autonomous driving in urban environment rely on a great variety of close-to-market visual sensors, which requires the fusion of the visual information provided by these sensors [3].

One of the most challenging issues is the fusion of 2D RGB imagery with other 3D range sensing modalities (*e.g.* Lidar) which can also be formulated as a camera calibration task. Internal calibration refers to the self parameters of the camera, while external parameters describe the *pose* of the camera with respect to a world coordinate frame. The problem becomes more difficult, when the RGB image is recorded with a non-conventional camera, such as central catadioptric or dioptric (*e.g.* fish-eye) panoramic cameras. Although such lenses have a more complex geometric model, their calibration also involves internal parameters and external pose. Recently, the geometric formulation of omnidirectional systems were extensively studied [16,1,5,13,23,24]. The internal calibration of such cameras depends on these geometric models. Although different calibration

methods and toolboxes exist [23,9,11] this problem is by far not trivial and is still in focus [24].

While internal calibration can be solved in a controlled environment, using special calibration patterns, pose estimation must rely on the actual images taken in a real environment. There are popular methods dealing with point correspondence estimation such as [23] or other fiducial marker images suggested in [9], which may be cumbersome to use in real life situations. This is especially true in a multimodal setting, when omnidirectional images need to be combined with other non-conventional sensors like lidar scans providing only range data. The Lidar-omnidirectional camera calibration problem was analyzed from different perspectives: in [21], the calibration is performed in natural scenes, however the point correspondences between the 2D-3D images are selected in a semi-supervised manner. [14] tackles calibration as an observability problem using a (planar) fiducial marker as calibration pattern. In [18], a fully automatic method is proposed based on mutual information (MI) between the intensity information from the depth sensor and the omnidirectional camera. Also based on MI, [27] performs the calibration using particle filtering. However, these methods require a range data with recorded intensity values, which is not always possible and often challenged by real-life lighting conditions.

This paper introduces a novel region based calibration framework for non-conventional 2D cameras and 3D lidar. Instead of establishing point matches or relying on artificial markers or recorded intensity values, we propose a pose estimation algorithm which works on segmented planar patches. Since segmentation is required anyway in many real-life image analysis tasks, such regions may be available or straightforward to detect. The main advantage of the proposed method is the use of regions instead of point correspondence and a generic problem formulation which allows to treat several types of cameras in the same framework. We reformulate pose estimation as a shape alignment problem, which is accomplished by solving a system of nonlinear equations based on the idea of [2]. However, the equations are constructed in a different way here due to the different dimensionality of the lidar and camera coordinate frames as well as the different camera model used for omnidirectional sensors. The method has been quantitatively evaluated on a large synthetic dataset and it proved to be robust and efficient in real-life situations.

2 Omnidirectional camera model

A unified model for central omnidirectional cameras was proposed by Geyer and Daniilidis [5], which represents central panoramic cameras as a projection onto the surface of a unit sphere. This formalism has been adopted and models for the internal projection function have been proposed by Micusik [13,12] and subsequently by Scaramuzza [22] who derived a general polynomial form of the internal projection valid for any type of omnidirectional camera. In this work, we will use the latter representation.

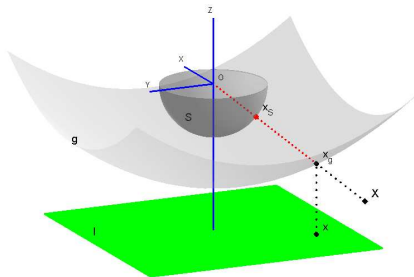


Fig. 1. Omnidirectional camera model

Let us first see the relationship between a point \mathbf{x} in the omnidirectional image \mathcal{I} and its representation on the unit sphere \mathcal{S} (see Fig. 1). Note that only the half sphere on the image plane side is actually used, as the other half is not visible from image points. Following [23,22], we assume that the camera coordinate system is in \mathcal{S} , the origin (which is also the center of the sphere) is the projection center of the camera and the z axis is the optical axis of the camera which intersects the image plane in the *principal point*. To represent the nonlinear (but symmetric) distortion of central omnidirectional optics, [23,22] places a surface g between the image plane and the unit sphere \mathcal{S} , which is rotationally symmetric around z . The details of the derivation of g can be found in [23,22]. Herein, as suggested by [23], we will use a fourth order polynomial $g(\|\mathbf{x}\|) = a_0 + a_2\|\mathbf{x}\|^2 + a_3\|\mathbf{x}\|^3 + a_4\|\mathbf{x}\|^4$ which has 4 parameters representing the internal parameters (a_0, a_2, a_3, a_4) of the camera (only 4 parameters as a_1 is always 0 [23]). The bijective mapping $\Phi: \mathcal{I} \rightarrow \mathcal{S}$ is composed of 1) lifting the image point $\mathbf{x} \in \mathcal{I}$ onto the g surface by an orthographic projection

$$\mathbf{x}_g = \begin{bmatrix} \mathbf{x} \\ a_0 + a_2\|\mathbf{x}\|^2 + a_3\|\mathbf{x}\|^3 + a_4\|\mathbf{x}\|^4 \end{bmatrix} \quad (1)$$

and then 2) centrally projecting the lifted point \mathbf{x}_g onto the surface of the unit sphere \mathcal{S} :

$$\mathbf{x}_S = \Phi(\mathbf{x}) = \frac{\mathbf{x}_g}{\|\mathbf{x}_g\|} \quad (2)$$

Thus the omnidirectional camera projection is fully described by means of unit vectors \mathbf{x}_S in the half space of \mathbb{R}^3 .

Let us see now how a 3D world point $\mathbf{X} \in \mathbb{R}^3$ is projected onto \mathcal{S} . This is basically a traditional central projection onto \mathcal{S} taking into account the extrinsic pose parameters, rotation \mathbf{R} and translation \mathbf{t} , acting between the camera (represented by \mathcal{S}) and world coordinate system. Thus for a world point \mathbf{X} and its image \mathbf{x} in the omnidirectional camera, the following holds on the surface of \mathcal{S} :

$$\Phi(\mathbf{x}) = \mathbf{x}_S = \Psi(\mathbf{X}) = \frac{\mathbf{R}\mathbf{X} + \mathbf{t}}{\|\mathbf{R}\mathbf{X} + \mathbf{t}\|} \quad (3)$$

3 Pose Estimation

Consider a Lidar camera with a 3D coordinate system having its origin in the center of laser sensor rotation, x and y axes pointing to the right and down, respectively, while z is pointing away from the sensor. Setting the world coordinate system to the Lidar’s coordinate system, we can relate a 3D Lidar point \mathbf{X} with its image \mathbf{x} in the omnidirectional camera using (3). In practical applications, like robot navigation or data fusion, the omnidirectional camera is usually calibrated (*i.e.* its intrinsic parameters (a_0, a_2, a_3, a_4) are known) and the relative pose (\mathbf{R}, \mathbf{t}) has to be estimated. Inspired by [25], we will reformulate pose estimation as a 2D-3D shape alignment problem. Our solution is based on the correspondence-less 2D shape registration approach of Domokos *et al.* [2], where non-linear shape deformations are recovered via the solution of a nonlinear system of equations. This method was successfully applied for a number of registration problems in different domains such as volume [20] or medical [15] image registration. In our case, however, the registration has to be done on the spherical surface \mathcal{S} , which requires a completely different way to construct equations.

Any corresponding (\mathbf{X}, \mathbf{x}) Lidar-omni point pair satisfies (3). Thus a classical solution of the pose estimation problem is to establish a set of such point matches using *e.g.* a special calibration target or, if lidar points contain also the laser reflectivity value, by standard intensity-based point matching, and solve for (\mathbf{R}, \mathbf{t}) . However, we are interested in a solution *without* a calibration target or correspondences because in many practical applications (*e.g.* infield mobile robot, autonomous driving systems), it is not possible to use a calibration target and most lidar sensors will only record depth information. Furthermore, lidar and camera images might be taken at different times and they need to be fused later based solely on the image content.

We will show that by identifying a single planar region both in the lidar and omni camera image, the extrinsic calibration can be solved. Since point correspondences are not available, (3) cannot be used directly. However, individual point matches can be integrated out yielding the following integral equation on the sphere \mathcal{S} :

$$\iint_{\mathcal{D}_S} \mathbf{x}_S d\mathcal{D}_S = \iint_{\mathcal{F}_S} \mathbf{z}_S d\mathcal{F}_S \quad (4)$$

\mathcal{D}_S and \mathcal{F}_S denote the surface patches on \mathcal{S} corresponding to the omni and lidar planar regions \mathcal{D} and \mathcal{F} , respectively. The above equation corresponds to a system of 2 equations, because a point on the surface \mathcal{S} has only 2 independent components. However, we have 6 pose parameters (3 rotation angles and 3 translation components). To construct a new set of equations, we adopt the general mechanism from [2] and apply a function $\omega : \mathbb{R}^3 \rightarrow \mathbb{R}$ to both sides of the equation, yielding

$$\iint_{\mathcal{D}_S} \omega(\mathbf{x}_S) d\mathcal{D}_S = \iint_{\mathcal{F}_S} \omega(\mathbf{z}_S) d\mathcal{F}_S \quad (5)$$

To get an explicit formula for the above integrals, the surface patches \mathcal{D}_S and \mathcal{F}_S can be naturally parameterized via Φ and Ψ over the planar regions \mathcal{D} and \mathcal{F} . Without loss of generality, we can assume that the third coordinate of $\mathbf{X} \in \mathcal{F}$ is 0, hence $\mathcal{D} \subset \mathbb{R}^2$, $\mathcal{F} \subset \mathbb{R}^2$; and $\forall \mathbf{x}_S \in \mathcal{D}_S : \mathbf{x}_S = \Phi(\mathbf{x}), \mathbf{x} \in \mathcal{D}$ as well as $\forall \mathbf{z}_S \in \mathcal{F}_S : \mathbf{z}_S = \Psi(\mathbf{X}), \mathbf{X} \in \mathcal{F}$ yielding the following form of (5):

$$\iint_{\mathcal{D}} \omega(\Phi(\mathbf{x})) \left\| \frac{\partial \Phi}{\partial x_1} \times \frac{\partial \Phi}{\partial x_2} \right\| dx_1 dx_2 = \iint_{\mathcal{F}} \omega(\Psi(\mathbf{X})) \left\| \frac{\partial \Psi}{\partial X_1} \times \frac{\partial \Psi}{\partial X_2} \right\| dX_1 dX_2 \quad (6)$$

where the magnitude of the cross product of the partial derivatives is known as the surface element. Adopting a set of nonlinear functions $\{\omega_i\}_{i=1}^{\ell}$, each ω_i generates a new equation yielding a system of ℓ independent equations. Although arbitrary ω_i functions could be used, power functions are computationally favorable [2] as these can be computed in a recursive manner:

$$\omega_i(\mathbf{x}_S) = x_1^{l_i} x_2^{m_i} x_3^{n_i}, \text{ with } 0 \leq l_i, m_i, n_i \leq 2 \text{ and } l_i + m_i + n_i \leq 3 \quad (7)$$

Algorithm 1 The proposed calibration algorithm.

Input: 3D point cloud and 2D omnidirectional binary image representing the same region, and the g coefficients

Output: External Parameters of the camera as \mathbf{R} and \mathbf{t}

- 1: Back-project the 2D image onto the unit sphere.
 - 2: Back-project the 3D template onto the unit sphere.
 - 3: Initialize the rotation matrix \mathbf{R} from the centroids of the shapes on the sphere.
 - 4: Initialize the translation \mathbf{t} by translating \mathcal{F} in the direction of its centroid until the area of \mathcal{F}_S and \mathcal{D}_S on the unit sphere are approximately equal.
 - 5: Construct the system of equations of (4) with the polynomial ω_i functions.
 - 6: Solve the set of nonlinear system of equations in (6) using the Levenberg-Marquardt algorithm
-

Hence we are able to construct an overdetermined system of 15 equations, which can be solved in the *least squares sense* via a standard *Levenberg-Marquardt* algorithm. The solution directly provides the pose parameters of the omni camera. To guarantee an optimal solution, initialization is also important. In our case, a good initialization ensures that the surface patches \mathcal{D}_S and \mathcal{F}_S overlap as much as possible. This is achieved by computing the centroids of the surface patches \mathcal{D}_S and \mathcal{F}_S respectively, and initializing \mathbf{R} as the rotation between them. Translation of the planar region \mathcal{F} will cause a scaling of \mathcal{F}_S on the spherical surface. Hence an initial \mathbf{t} is determined by translating \mathcal{F} along the axis going through the centroid of \mathcal{F}_S such that the area of \mathcal{F}_S becomes approximately

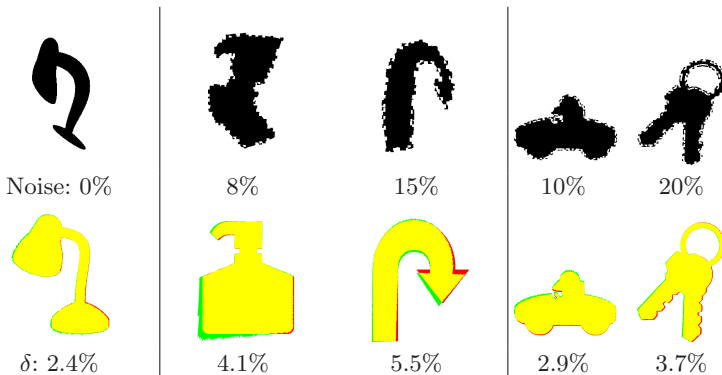


Fig. 2. Examples of various amount of simulated segmentation errors. First column contains a result without such errors, the next two show segmentation errors on the omnidirectional image, while the last two on the 3D planar region. The second row shows the δ error and the backprojected shapes overlaid in green and red colors. (best viewed in color)

equal to that of \mathcal{D}_S . The summary of the proposed algorithm with the projection on the unit sphere is presented in Algorithm 1.

4 Evaluation on synthetic data

For the quantitative evaluation of the proposed method, we generated a benchmark set using 30 different shapes as 3D planar regions and their omnidirectional images taken by a virtual camera, a total of 150 2D-3D data pairs. The synthetic omni images were generated by a virtual camera being randomly rotated in the range of $(-40^\circ \cdots 40^\circ)$ and randomly translated in the range of $(0 \cdots 200)$. Assuming that the planar shape on the 800×800 template image represents a $5m \times 5m$ planar patch in 3D space, the $(0 \cdots 200)$ translation is equivalent to $(0 \cdots 1.25)$ meter in metric coordinates.

In practice, the planar regions used for calibration are segmented out from the lidar and omni images. In either case, we cannot produce perfect shapes, therefore robustness against segmentation errors was also evaluated on simulated data (see samples in Fig. 2): we randomly added or removed squares uniformly around the boundary of the shapes, both in the omni images and on the 3D planar regions, yielding a segmentation error of 5% -20% of the original shape.

The algorithm was implemented in Matlab and all experiments were run on a standard quad-core PC. Quantitative comparisons in terms of the various error plots are shown in Fig. 3, Fig. 4, and Fig. 5 (each test case is sorted independently in a best-to-worst sense). Calibration errors were characterized in terms of the percentage of non-overlapping area of the reference 3D shape and the backprojected omni image (denoted by δ in Fig. 5), as well as the error in each of the estimated pose parameters given in degrees in Fig. 4 and in cm in

Fig. 3. Note that our method is quite robust against segmentation errors up to 15% error level.

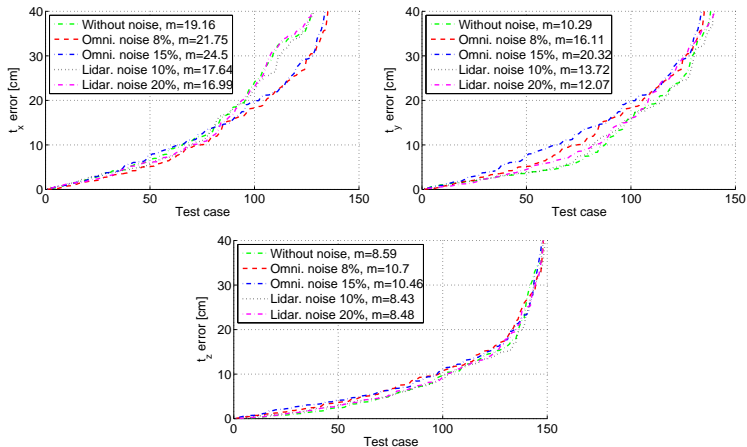


Fig. 3. Translation errors in cm along the x , y , and z axis. m denotes median error, *Omni noise* and *Lidar noise* stand for segmentation error on the omni and 3D regions, respectively (best viewed in color).

5 Experimental validation

For the experimental validation of the proposed algorithm, two different omnidirectional camera setups are shown. In order to fuse the omnidirectional camera data and the lidar scan both the internal and external parameters are needed. The internal parameters of the omnidirectional camera were determined using the toolbox of [23]. Note that this internal calibration needs to be performed only once for a camera. The external parameters are then computed using the proposed algorithm.

5.1 Region segmentation

In order to make the pose estimation user friendly, the region selection both in 2D and 3D was automated with efficient segmentation algorithms.

There are several automated or semi-automated 2D segmentation algorithms in the literature including clustering, histogram thresholding, energy based or region growing variants [28]. In this work we used a simple region growing algorithm which proved to be robust enough in urban environment [19].

For the 3D segmentation a number of point cloud segmentation methods are available, including robust segmentation [17] or difference of normals based

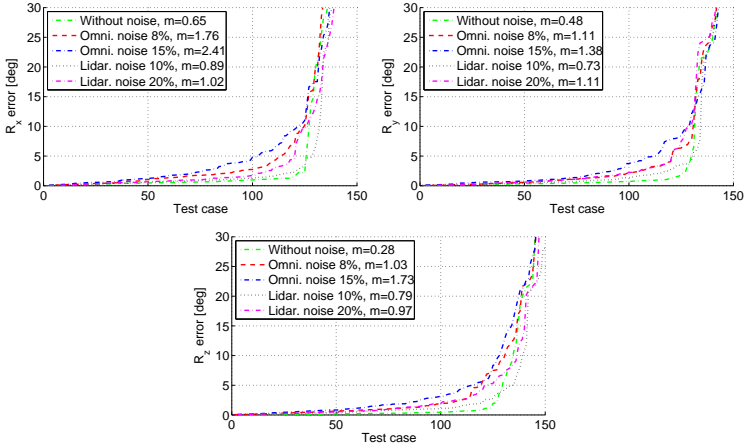


Fig. 4. Rotation errors in degrees along the x , y , and z axis. m denotes median error, *Omni noise* and *Lidar noise* stand for segmentation error on the omni and 3D regions, respectively (best viewed in color).

segmentation[7]. Like in 2D, region growing gave stable results in our test cases thus it was suitable for the fusion algorithm as to extract planar input regions. This segmentation algorithm is based on a set composition principle, *i.e.* an initial starting point (seed) is selected from the original point cloud, and iteratively the set is completed with neighbor points which have similar normal (within a certain threshold limit c_θ), or their curvature is less than a specified curvature threshold c_t .

Considering the correspondence establishment between the segmented 2D and 3D regions as minimal one-click user intervention, this aspect represents the only human interaction in the current procedure. After the first 2D-3D region pair establishment, further ones can easily be added by searching with a sample consensus approach for the neighbor plain patches. We remark, that a fully automatic region correspondence could be implemented by detecting and extracting windows [6] (see *e.g.* Fig. 7) which are typically planar and present in urban scenes.

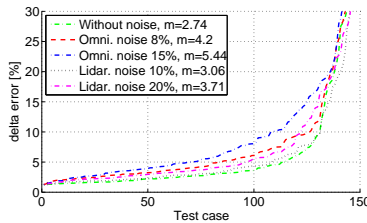


Fig. 5. Backprojection (δ) errors. (best viewed in color)

5.2 Urban data fusion results

The input data with the segmented regions as well as the results are shown in Fig. 6 and Fig. 7 for a catadioptric-lidar and dioptric-lidar camera pairs respectively. The omnidirectional images were captured with a commercial SLR camera with a catadioptric lens (Fig. 6) and a fish-eye (Fig. 7) respectively. For the 3D range data, a custom lidar was used in Fig. 6 to acquire data similar to the one described in [26] with an angular resolution up to half degree and a depth accuracy of 1cm . In Fig. 7, the 3D point cloud was recorded by a Velodyne Lidar mounted on a moving car [8].

After the raw data acquisition, the segmentation was performed in both domains. For the 3D data, segmentation yields a parametric equation and boundaries of the selected planar region. This was then uniformly sampled to get a dense homogeneous set of points (*i.e.* we do not rely on the Lidar resolution after segmentation), which was subsequently transformed with a rigid motion $(\mathbf{R}_0, \mathbf{t}_0)$ into the $Z = 0$ plane yielding appropriate point coordinates \mathbf{X} used in the right hand side of (6). The \mathbf{x} points of the left hand side of (6) are fed with the pixel coordinates of the segmented omnidirectional image.

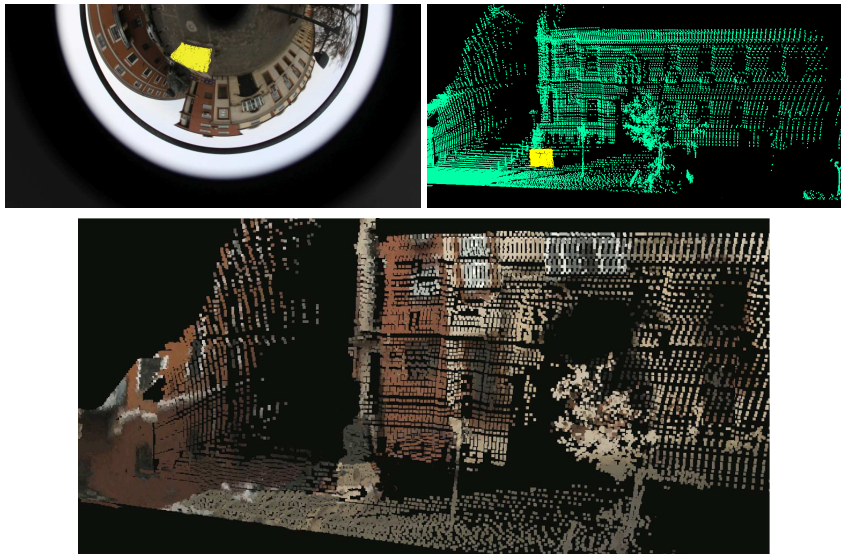


Fig. 6. Catadioptric and lidar images with segmented area marked in yellow, and the fused images after pose estimation. (best viewed in color)

Once the output (\mathbf{R}, \mathbf{t}) is obtained from Algorithm 1, the final transformation acting between the lidar and omni camera can then be computed as a composite rigid transformation of $(\mathbf{R}_0, \mathbf{t}_0)$ and (\mathbf{R}, \mathbf{t}) . The final computed transformation was used to fuse the depth and RGB data by reprojecting the point cloud on

the image plane using the internal and external camera parameters, and thus obtaining the color for each point of the 3D point cloud. The method proved to be robust against segmentation errors, but a sufficiently large overlap between the regions is required for better results.

Acknowledgment

This research was partially supported by the European Union and the State of Hungary, co-financed by the European Social Fund through projects TAMOP-4.2.4.A/2-11-1-2012-0001 National Excellence Program and FuturICT.hu (grant no.: TAMOP-4.2.2.C-11/1/KONV-2012-0013); as well as by Domus MTA Hungary. The authors gratefully acknowledge the help of Csaba Benedek from DEVA Lab., SZTAKI in providing us with preprocessed Velodyne Lidar scans, as well as the discussions with Radu Orghidan and Cedric Demonceaux in the early stage of this work. The catadioptric camera was provided by the Multimedia Technologies and Telecommunications Research Center of UTCN with the help of Camelia Florea.

6 Conclusions

In this paper a new method for pose estimation of non-conventional cameras is proposed. The method is based on a point correspondence-less registration technique, which allows reliable estimation of extrinsic camera parameters. The algorithm was quantitatively evaluated on a large synthetic data set and proved to be robust on real data fusion as well.

References

1. Baker, S., Nayar, S.K.: A Theory of Single-Viewpoint Catadioptric Image Formation. *International Journal of Computer Vision* 35(2), 175–196 (1999)
2. Domokos, C., Nemeth, J., Kato, Z.: Nonlinear Shape Registration without Correspondences. *IEEE Transactions on Pattern Analysis and Machine Intelligence* 34(5), 943–958 (2012)
3. Furgale, P.T., Schwesinger, U., Rufi, M., Derendarz, W., Grimmer, H., Muehlfeiler, P., Wonneberger, S., Timpner, J., Rottmann, S., Li, B., Schmidt, B., Nguyen, T.N., Cardarelli, E., Cattani, S., Bruning, S., Horstmann, S., Stellmacher, M., Mielenz, H., Köser, K., Beermann, M., Hane, C., Heng, L., Lee, G.H., Fraundorfer, F., Iser, R., Triebel, R., Posner, I., Newman, P., Wolf, L.C., Pollefeys, M., Brosig, S., Effertz, J., Pradalier, C., Siegwart, R.: Toward automated driving in cities using close-to-market sensors: An overview of the V-Charge Project. In: *Intelligent Vehicles Symposium*. pp. 809–816. Gold Coast City, Australia (June 2013)
4. Geiger, A., Lauer, M., Wojek, C., Stiller, C., Urtasun, R.: 3D Traffic Scene Understanding From Movable Platforms. *IEEE Transactions on Pattern Analysis and Machine Intelligence* 36(5), 1012–1025 (2014)

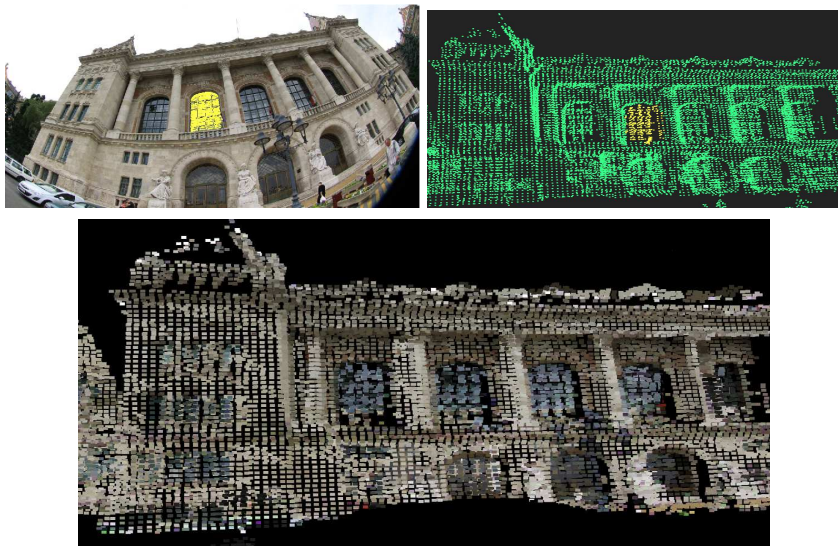


Fig. 7. Dioptric (fisheye) and lidar images with segmented area marked in yellow, and the fused images after pose estimation. (best viewed in color)

5. Geyer, C., Daniilidis, K.: A unifying theory for central panoramic systems. In: European Conference on Computer Vision. pp. 445–462. Dublin, Ireland (June 2000)
6. Goron, L., Tamas, L., Reti, I., Lazea, G.: 3D laser scanning system and 3D segmentation of urban scenes. In: Automation Quality and Testing Robotics Conference. vol. 1, pp. 81–85. IEEE, Cluj-Napoca, Romania (May 2010)
7. Ioannou, Y., Taati, B., Harrap, R., Greenspan, M.: Difference of Normals as a Multi-scale Operator in Unorganized Point Clouds. In: International Conference on 3D Imaging, Modeling, Processing, Visualization and Transmission. pp. 501–508. IEEE Computer Society, Los Alamitos, CA, USA (September 2012)
8. Józsa, O., Börcs, A., Benedek, C.: Towards 4D virtual city reconstruction from Lidar point cloud sequences. In: ISPRS Workshop on 3D Virtual City Modeling, ISPRS Annals of Photogrammetry, Remote Sensing and the Spatial Information Sciences, vol. II-3/W1, pp. 15–20. Regina, Canada (2013)
9. Kannala, J., Brandt, S.S.: A Generic Camera Model and Calibration Method for Conventional, Wide-Angle, and Fish-Eye Lenses. *IEEE Transactions on Pattern Analysis and Machine Intelligence* 28(8), 1335–1340 (2006)
10. Lin, D., Fidler, S., Urtasun, R.: Holistic Scene Understanding for 3D Object Detection with RGBD Cameras. In: International Conference on Computer Vision. pp. 1417–1424. IEEE Computer Society, Sydney, Australia (December 2013)
11. Mei, C., Rives, P.: Single View Point Omnidirectional Camera Calibration from Planar Grids. In: International Conference on Robotics and Automation. pp. 3945–3950. Roma, Italy (April 2007)
12. Mičušík, B.: Two-View Geometry of Omnidirectional Cameras. Phd thesis, Department of Cybernetics, Faculty of Electrical Engineering, Czech Technical University, Prague, Czech Republic (June 2004)

13. Mičušík, B., Pajdla, T.: Para-catadioptric Camera Auto-calibration from Epipolar Geometry. In: Asian Conference on Computer Vision. vol. 2, pp. 748–753. Seoul, Korea South (January 2004)
14. Mirzaei, F.M., Kottas, D.G., Roulletiotis, S.I.: 3D LIDAR-camera intrinsic and extrinsic calibration: Identifiability and analytical least-squares-based initialization. *International Journal of Robotics Research* 31(4), 452–467 (2012)
15. Mitra, J., Kato, Z., Marti, R., Oliver, A., Lladó, X., Sidibé, D., Ghose, S., Vilanova, J.C., Comet, J., Meriaudeau, F.: A Spline-based Non-linear Diffeomorphism for Multimodal Prostate Registration. *Medical Image Analysis* 16(6), 1259–1279 (2012)
16. Nayar, S.K.: Catadioptric Omnidirectional Camera. In: Conference on Computer Vision and Pattern Recognition. pp. 482–488. Washington, USA (June 1997)
17. Nurunnabi, A., Belton, D., West, G.: Robust Segmentation in Laser Scanning 3D Point Cloud Data. In: Digital Image Computing Techniques and Applications. pp. 1–8. Fremantle, Australia (December 2012)
18. Pandey, G., McBride, J.R., Savarese, S., Eustice, R.M.: Automatic Targetless Extrinsic Calibration of a 3D Lidar and Camera by Maximizing Mutual Information. In: AAAI National Conference on Artificial Intelligence. pp. 2053–2059. Toronto, Canada (July 2012)
19. Preetha, M., Suresh, L., Bosco, M.: Image Segmentation using Seeded Region Growing. In: Computing, Electronics and Electrical Technologies. pp. 576–583. Nagercoil, India (March 2012)
20. Santa, Z., Kato, Z.: Correspondence-Less Non-rigid Registration of Triangular Surface Meshes. In: Conference on Computer Vision and Pattern Recognition. pp. 2275–2282. IEEE Computer Society, Portland, Oregon, USA (June 2013)
21. Scaramuzza, D., Harati, A., Siegwart, R.: Extrinsic Self Calibration of a Camera and a 3D Laser Range Finder from Natural Scenes. In: International Conference on Intelligent Robots and Systems. pp. 4164–4169. San Diego, USA (October 2007)
22. Scaramuzza, D., Martinelli, A., Siegwart, R.: A Flexible Technique for Accurate Omnidirectional Camera Calibration and Structure from Motion. In: International Conference on Computer Vision Systems. pp. 45–51. Washington, USA (January 2006)
23. Scaramuzza, D., Martinelli, A., Siegwart, R.: A Toolbox for Easily Calibrating Omnidirectional Cameras. In: International Conference on Intelligent Robots and Systems. pp. 5695–5701. Beijing, China (October 2006)
24. Schoenbein, M., Strauss, T., Geiger, A.: Calibrating and Centering Quasi-Central Catadioptric Cameras. In: International Conference on Robotics and Automation. pp. 1253–1256. Hong-Kong, China (June 2014)
25. Tamas, L., Kato, Z.: Targetless Calibration of a Lidar - Perspective Camera Pair. In: International Conference on Computer Vision, Bigdata3dev Workshops. pp. 668–675. Sydney, Australia (December 2013)
26. Tamas, L., Majdik, A.: Heterogeneous Feature Based Correspondence Estimation. In: Multisensor Fusion and Integration for Intelligent Systems. pp. 89–94. IEEE, Hamburg, Germany (June 2012)
27. Taylor, Z., Nieto, J.: A Mutual Information Approach to Automatic Calibration of Camera and Lidar in Natural Environments. In: Australian Conference on Robotics and Automation. pp. 3–8. Wellington, Australia (December 2012)
28. Vantaram, S.R., Saber, E.: Survey of Contemporary Trends in Color Image Segmentation. *Journal of Electronic Imaging* 21(4), 1–28 (2012)